MPMI Vol. 37, No. 4, 2024, pp. 396–406, https://doi.org/10.1094/MPMI-05-23-0068-R

Three-Dimensional Ultrastructure of *Arabidopsis* Cotyledons Infected with *Colletotrichum higginsianum*

Kamesh C. Regmi,[1,†] Suchismita Ghosh,[1] Benjamin Koch,[1] Ulla Neumann,[2] Barry Stein,[1] Richard J. O'Connell,[3] and Roger W. Innes[1]

[1] Indiana University, Department of Biology, Bloomington, IN 47405, U.S.A.
[2] Max Planck Institute for Plant Breeding Research, 50829 Cologne, Germany
[3] Université Paris-Saclay, INRAE, UR BIOGER, 91120 Palaiseau, France

Accepted for publication 18 December 2023.

We used serial block-face scanning electron microscopy (SBF-SEM) to study the host–pathogen interface between *Arabidopsis* cotyledons and the hemibiotrophic fungus *Colletotrichum higginsianum*. By combining high-pressure freezing and freeze-substitution with SBF-SEM, followed by segmentation and reconstruction of the imaging volume using the freely accessible software IMOD, we created 3D models of the series of cytological events that occur during the *Colletotrichum–Arabidopsis* susceptible interaction. We found that the host cell membranes underwent massive expansion to accommodate the rapidly growing intracellular hypha. As the fungal infection proceeded from the biotrophic to the necrotrophic stage, the host cell membranes went through increasing levels of disintegration culminating in host cell death. Intriguingly, we documented autophagosomes in proximity to biotrophic hyphae using transmission electron microscopy (TEM) and a concurrent increase in autophagic flux between early to mid/late biotrophic phase of the infection process. Occasionally, we observed osmiophilic bodies in the vicinity of biotrophic hyphae using TEM only and near necrotrophic hyphae under both TEM and SBF-SEM. Overall, we established a method for obtaining serial SBF-SEM images, each with a lateral (*x-y*) pixel resolution of 10 nm and an axial (*z*) resolution of 40 nm, that can be reconstructed into interactive 3D models using the IMOD. Application of this method to the *Colletotrichum–Arabidopsis* pathosystem allowed us to more fully understand the spatial arrangement and morphological architecture of the fungal hyphae after they penetrate epidermal cells of *Arabidopsis* cotyledons and the cytological changes the host cell undergoes as the infection progresses toward necrotrophy.

†Corresponding author: K. C. Regmi; regmi1@kenyon.edu

Current address for K. C. Regmi: Kenyon College, Gambier, OH 43022.

Funding: This research was funded by the U.S. National Science Foundation Division of Integrative Organismal Systems Plant Biotic Interactions and Plant Genome Research programs (award nos. IOS-1645745, IOS-1842685, and IOS-2141969) and the U.S. Department of Energy Office of Biological and Environmental Research (DE-SC0020348). S. Ghosh and B. Koch were supported by a Carlos Miller fellowship from the Indiana University Foundation.

***e*-Xtra:** Supplementary material is available online.

The author(s) declare no conflict of interest.

Keywords: *Arabidopsis thaliana*, *Colletotrichum higginsianum*, ER bodies, IMOD, macroautophagy, serial block-face scanning electron microscopy, three-dimensional reconstruction

The *Colletotrichum* genus of ascomycete fungal pathogens comprises more than 280 species and attacks a diverse array of dicot and monocot plant species globally (Crous et al. 2004; Liu et al. 2022). Infection starts with a transient biotrophic phase, in which the fungus first penetrates the cell wall of epidermal cells and invaginates the host cell plasma membrane (PM), forming biotrophic hyphae that extract nutrients without rupturing the host PM. This is followed by a necrotrophic phase, in which the fungus invades neighboring cells and causes cell death and tissue destruction (Bailey et al. 1992; Heath 1983; Latunde-Dada et al. 1996; O'Connell et al. 2012). As such, these pathogenic fungi are referred to as hemibiotrophs (Luttrell 1974). More recently, the classification of fungal trophic behavior based on a genome-wide analysis of carbohydrate-active enzyme genes placed *Colletotrichum* species into a new category called "intracellular (appressorial) mesotrophs" (Hane et al. 2020). Among various host–parasite pathosystems, the infection of *Arabidopsis thaliana* by *Colletotrichum higginsianum* is considered a model hemibiotrophic system for studying the cellular and molecular bases of fungal pathogenicity (Bailey et al. 1992; O'Connell et al. 2004).

With the advent of transmission electron microscopy (TEM) and associated biological fixation techniques, many ultrastructural studies of plant–pathogen interactions have yielded a significant body of cell biological knowledge (Faoro et al. 2022). Specifically, *Colletotrichum* pathogenesis has been studied at the ultrastructural level in a range of hemibiotrophic interactions, including *C. gloeosporioides*–tangerine (Brown 1977), *C. lindemuthianum*–bean (O'Connell 1987), *C. lagenarium*–cucumber (Xuei et al. 1988), *C. sublineola*–sorghum (Wharton et al. 2001), *C. destructivum*–cowpea (Latunde-Dada et al. 1996), *C. trifolii*–alfalfa (Mould et al. 1991), *C. graminicola*–maize (Mims and Vaillancourt 2002), and *C. higginsianum*–*Arabidopsis* (Kleemann et al. 2012; O'Connell et al. 2004). The *Colletotrichum* conidia germinate on the plant surface to produce germ tubes that develop into domed, melanized structures called appressoria that penetrate the host epidermal cell by means of a thin penetration peg (Brown 1977; Latunde-Dada et al. 1996; Mims and Vaillancourt 2002; O'Connell 1987; Wharton et al. 2001; Xuei et al. 1988). Upon successful penetration, *C. sublineola*, *C. lagenarium*, *C. lindemuthianum*, and *C. graminicola* have been reported to induce the formation of localized callose deposits called papillae at penetration sites. However, these do not

prevent the fungi from producing inside living epidermal cells large-diameter bulbous intracellular hyphae that are surrounded by the intact host PM and are characteristic of the biotrophic phase of infection (Mims and Vaillancourt 2002; O'Connell et al. 1985; Wharton et al. 2001; Xuei et al. 1988).

During the biotrophic phase of *Colletotrichum* species, nutrients move from the host to the fungus, crossing both the host and fungal PMs. The space between these two membranes is referred to as the interfacial matrix and is recognized as a site of vesicular traffic and signal exchange between the fungal and the plant cells in both symbiotic (Ivanov et al. 2019; Roth et al. 2019) and biotrophic interactions (Micali et al. 2011; Mims et al. 2004; Voegele and Mendgen 2003). The interfacial matrix surrounding *C. lindemuthianum* biotrophic hyphae is enriched in polysaccharides, with the adjacent host cell cytoplasm enriched in Golgi and vesicles (O'Connell 1987). Localized patches of interfacial matrix called interfacial bodies have been reported around the biotrophic hyphae of *C. higginsianum* and have been shown to contain secreted effector proteins (Kleemann et al. 2012). During the biotrophic phase of infection, the host cell membranes and organelles also maintain their structural integrity (Brown 1977; Mims and Vaillancourt 2002; O'Connell 1987; Wharton et al. 2001; Xuei et al. 1988). However, as these fungi enter the necrotrophic phase, the host cell membranes degenerate, and thinner necrotrophic hyphae radiate into neighboring cells and intercellular spaces. The macroscopic anthracnose disease symptoms usually become visible at this stage (Mims and Vaillancourt 2002).

Although the cited studies have provided snapshots of *Colletotrichum* sp. infection processes, 2D electron micrographs provide an incomplete representation of the inherently 3D fungal structures, and this drawback is particularly problematic for complex structures such as biotrophic and necrotrophic fungal hyphae. Here, we combined cryofixation by high-pressure freezing (HPF) and serial block-face scanning electron microscopy (SBF-SEM) to study the postpenetration events in the *A. thaliana–C. higginsianum* pathosystem. Since its inception, the combination of backscattering contrast obtained from block faces and a custom-designed ultramicrotome has allowed SBF-SEM to greatly expand the field of 3D volumetric ultrastructural imaging of biological structures (Denk and Horstmann 2004). We reconstructed models based on 3D datasets of this host–pathogen interaction at both the biotrophic and necrotrophic phases, and found that during the biotrophic phase of infection, the intracellular hypha displaces a considerable host cell volume and this displacement is concomitant with large-scale expansion of host cell membranes. Notably, during mid/late biotrophy, we observed autophagosomes in host cells in proximity to fungal hyphae, which was concurrent with an increase in autophagic flux, indicating that macroautophagy is highly active near infection sites during mid/late biotrophy. The transition toward necrotrophy was accompanied by a progressive deterioration of host cell membranes, and upon reaching the necrotrophic phase of infection, the fungal hyphae had extensively radiated through the host tissue and the hyphae formed a single, multinucleate interconnected structure that frequently spanned intercellular spaces between cells.

Results

Early biotrophic phase

To generate 3D images of fungal infection sites, we used SBF-SEM. In brief, *Arabidopsis* cotyledons were infected with *C. higginsianum* and then entire cotyledons were collected at approximately 52 h postinoculation (hpi) and high-pressure frozen, which was followed by freeze-substitution, staining, and embedding in resin (see "Materials and Methods"). Sample blocks were then imaged using a Teneo VolumeScope SBF-SEM. The infected cells shown in Figure 1A and B are the 103rd and 1st images from the same SBF-SEM image stack. In the cell boxed in Figure 1A and D (Supplementary Video S1), the hyphae occupy a large volume of the epidermal cell (Fig. 1C) and have largely displaced the central vacuole, but both the tonoplast and the PM remain intact (Fig. 1D; Supplementary Video S2). When observed through an 8-μm depth and reconstructed in 3D (200 sections; 40 nm per slice), biotrophic intracellular hyphae were shown to be pear-shaped (cyan; Fig. 1C; Supplementary Video S2) or horn-shaped (yellow in Fig. 1C and Supplementary Video S2). The biotrophic hyphae marked with white arrowheads in Figure 1A and B were much more electron-dense than the hyphae marked with black arrowheads in Figure 1A. We speculate that the removal of the appressorium during HPF caused a direct influx of freeze-substitution fluid into the darkly stained hypha through the exposed penetration peg (Fig. 1B), causing more intense osmication. As seen in Supplementary Video S1 and reconstructed in Figure 1C and Supplementary Video S2, the lightly osmicated hypha (yellow in Fig. 1C and Supplementary Video S2) is visibly more developed than the highly osmicated one (cyan in Fig. 1C and Supplementary Video S2), suggesting that the penetration peg was already sealed by a septum. We also observed vesicular structures interspersed in the plant cytoplasm that were found to be vesiculo-tubular structures when imaged in 3D (red in Fig. 1E and Supplementary Video S3). We speculate that these may represent the beginning of vacuolar fragmentation that becomes extensive at later stages of infection, as described below (see "Mid-biotrophic phase"). Numerous oval structures were also evident in the infected epidermal cell that were reminiscent of the dilated endoplasmic reticulum (ER) cisternae called ER bodies (indicated by asterisks in Fig. 1D) (Gunning 1998; Hayashi et al. 2001; Matsushima et al. 2003a). When visualized in three-dimensions, these cigar-shaped ER bodies in fact formed interconnected stacks (colored blue in Fig. 1E), something not easily deduced from the series of 2D micrographs.

Mid-biotrophic phase

At 52 hpi, we also found evidence for a more advanced level of membrane disintegration in the infected host cell. The cells shown in Figure 2A and B are the 241st and 1st images from a single SBF-SEM image stack. In two adjacent epidermal cells, both infected with *C. higginsianum*, two different stages of membrane fragmentation are evident (Fig. 2A and B; Supplementary Video S4). In the epidermal cell to the left (Fig. 2A, boxed region magnified in Fig. 2C), both the vacuolar and PMs were still intact (Fig. 2C, showing intact vacuole colored in light ochre), akin to what was observed in Figure 1D and G and Supplementary Video S1. Moreover, other organelles, including the nucleus, chloroplast, and mitochondria, also maintained their structural integrity (Supplementary Video S4). As such, we inferred that the fungus was still in its biotrophic stage.

By contrast, the central vacuole in the epidermal cell to the right had undergone major changes (Fig. 2B, boxed region magnified in Fig. 2D). The central vacuole of the epidermal cell shown in Figure 2D and Supplementary Video S4 shows a profusion of membrane invaginations and vesicles inside the lumen (arrowheads and arrows, respectively), marking a more advanced stage of disease progression. These infoldings of the tonoplast, engulfment of cytoplasm by the vacuole, and scission of vesicles into the vacuolar lumen are reminiscent of the ultrastructural details of microautophagy described by Hiratsuka and Terasaka (2011) in nucellar cells of *Pinus densiflora* (Hiratsuka and Terasaka 2011; Hiratsuka et al. 2002; Marshall and Vierstra 2018; van Doorn and Woltering 2005). However, we cannot definitively claim that the aforementioned features are

indicative of a cell undergoing microautophagy en route to programmed cell death. Through manual segmentation, we were able to generate 3D reconstructions of the two infected adjacent cells (Fig. 2E and F; Supplementary Video S5), but accurate manual segmentation of the numerous membrane features throughout the 275 serial micrographs proved impractical. Hence, we used the isosurface tool in IMOD to automate the segmentation of these membranes, which helped us juxtapose the level of membrane disintegration between the two adjoining epidermal cells. In IMOD, an isosurface is a surface superimposed on pixels where the intensity values exceed a threshold value set by the user. At the threshold intensity levels used here, we were able to accurately model the membrane fragments throughout the 11-µm imaging depth, which allowed us to generate isosurface 3D models that clearly show that the epidermal cell shown in Figure 2D (Supplementary Video S6) had a higher level of membrane fragmentation than its neighboring cell shown in Figure 2C (Supplementary Video S7).

Mid/late biotrophic phase and evidence for macroautophagy

Although we could not conclusively establish that microautophagy was occurring during the mid-biotrophic phase of *C. higginsianum* infection in *Arabidopsis* Col-0 plants, we found ultrastructural evidence of macroautophagy during the mid/late biotrophic phase of *C. higginsianum* infection in *Arabidopsis Ler-0* leaves, as shown by the presence of numerous double-membraned vesicles adjacent to biotrophic hyphae (Fig. 3A to E). These structures appear to be autophagosomes, which have previously been shown to accumulate around haustoria (functionally equivalent to biotrophic hyphae) formed by the oomycete pathogen *Phytophthora infestans* during infection of *Nicotiana benthamiana* leaf cells (Dagdas et al. 2018). Notably, knockdown of a gene encoding an autophagy cargo receptor, *Joka2*, in *N. benthamiana* enhances susceptibility to *P. infestans* (Dagdas et al. 2016), suggesting that autophagy plays a central role in immune responses.

Given our ultrastructural evidence for macroautophagy during *C. higginsianum* pathogenesis, we hypothesized that an increase in autophagic flux would coincide with this mid/late biotrophic phase of infection. Autophagic flux can be measured using the green fluorescent protein (GFP)-ATG8 processing assay by evaluating the ratio between GFP-ATG8 and free GFP, wherein free GFP is released upon proteolysis of GFP-ATG8 in the vacuole (Bassham 2015; Klionsky et al. 2021; Shin et al. 2014; Torggler et al. 2017). We monitored relative levels of GFP-ATG8a and free GFP proteins in 7-day-old *Arabidopsis* Col-0 seedlings infected with *C. higginsianum*, beginning at 24 hpi (Fig. 3F). GFP-ATG8a increased during infection, reaching a maximum level between 56 and 60 hpi, while free GFP showed a visibly significant increase from 52 to 60 hpi as well (Fig. 3F). Importantly, the mock-inoculated controls show virtually no free GFP from 24 to 60 hpi and show stable expression of GFP-ATG8a. To perform a semiquantitative analysis of the autophagy flux assay, the ratio

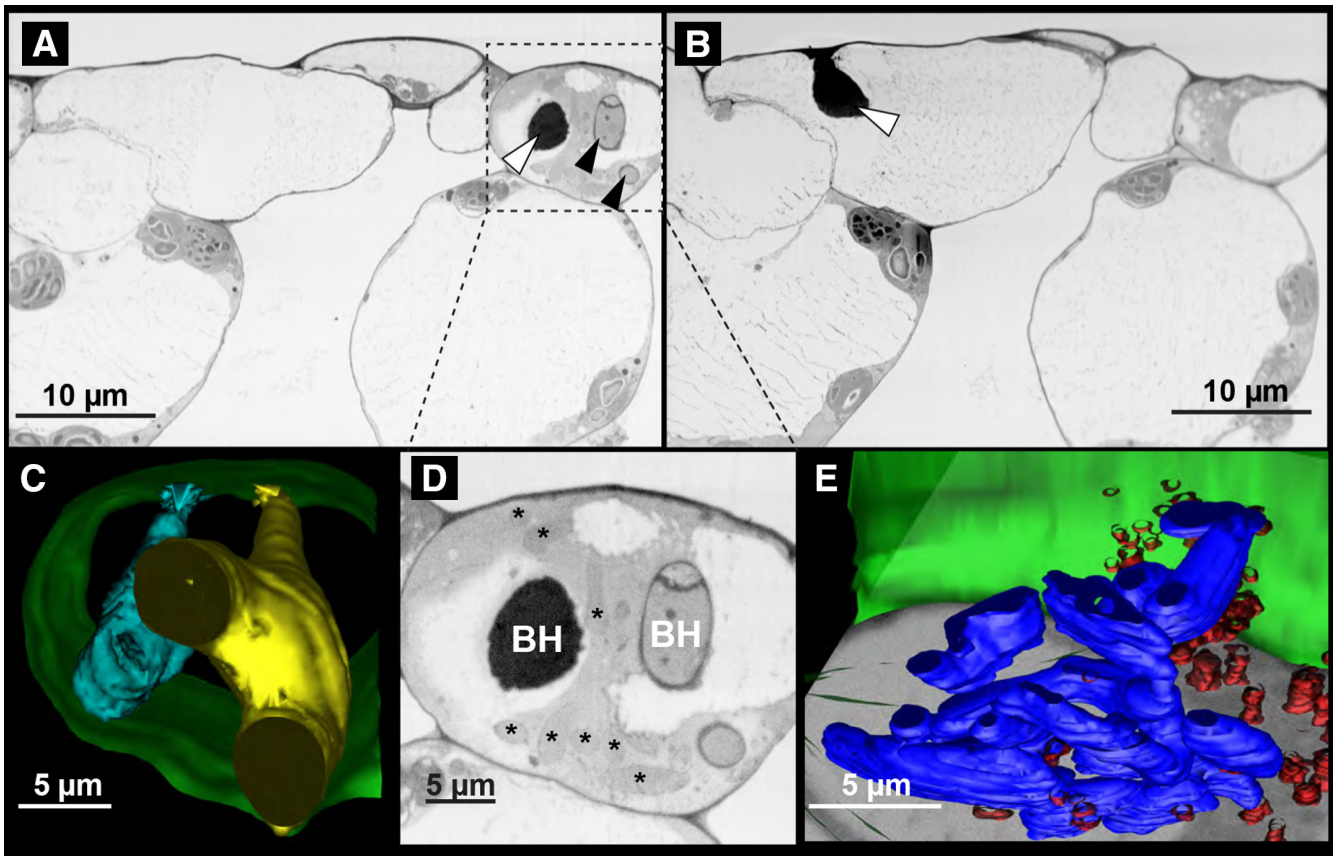

Fig. 1. Serial block-face scanning electron microscopy (SBF-SEM) imaging of the biotrophic phase of *Arabidopsis* cotyledon epidermal cells infected with *Colletotrichum higginsianum.* **A,** The 103rd and **B,** 1st micrographs from a single SBF-SEM image stack containing 200 images, showing primary intracellular hyphae (arrowheads) in the epidermal cells. The hyphae marked with white arrowheads were more intensely osmicated than the ones marked with black arrowheads. **C,** A 3D model of two adjacent intracellular hyphae (cyan and yellow) in the epidermal cell (green, cell wall) that corresponds to the entire volume of the cell boxed in A. **D,** Cropped and digitally enlarged micrograph from A showing biotrophic hyphae (BH) and endoplasmic reticulum (ER) bodies (asterisks). **E,** A 3D reconstruction showing the interconnected stacks of ER bodies (blue) and vesiculo-tubular membrane-bound structures (red), also from the entire volume of the cell boxed in A and shown in E. Please refer to Supplementary Videos S1 to S3 to see entire stacks and complete 3D models.

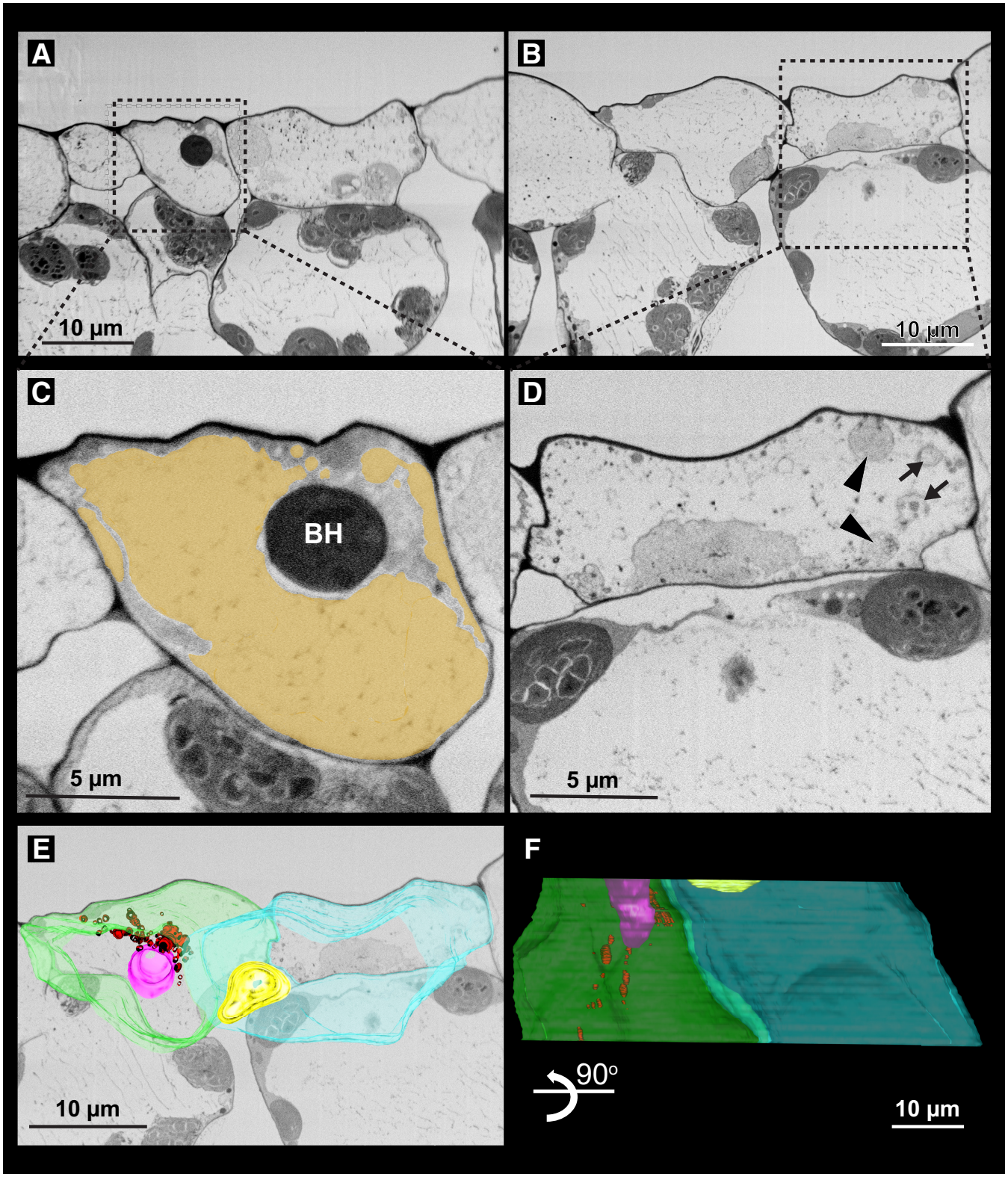

Fig. 2. Increased membrane disintegration during *Colletotrichum higginsianum* infection of Col-0. **A,** The 241st and **B,** 1st serial block-face scanning electron microscopy (SBF-SEM) images from a single stack containing 275 micrographs. **C,** Boxed and digitally magnified image from A showing a biotrophic hypha (BH) and the intact vacuole (light ochre) in the host epidermal cell. **D,** Engulfment of the cytoplasm (arrowheads) and vesicles (arrows) in the vacuolar lumen at 52 h postinoculation (hpi). **E,** A 3D reconstruction of the biotrophic hyphae (yellow and magenta) in the two adjacent epidermal cells shown in A and B (light blue and green) superimposed on a grayscale SBF-SEM image. **F,** A 3D model from E rotated 90°. For a comparison between the level of membrane disintegration between the cell depicted in A versus the cell depicted in B, please refer to Supplementary Videos S6 and S7.

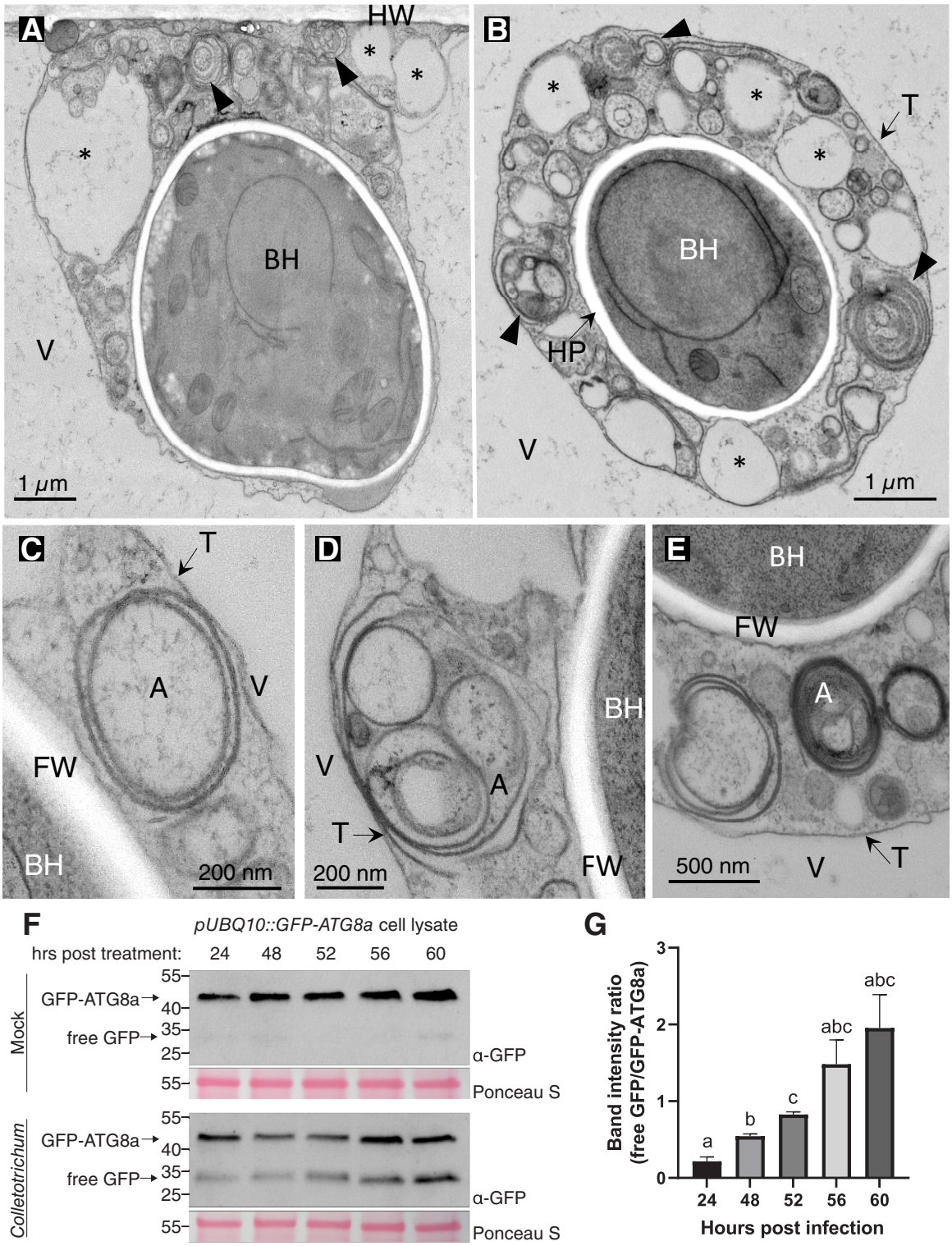

Fig. 3. Macroautophagy during mid/late biotrophic phase of *Colletotrichum higginsianum* infection. Transmission electron micrographs showing *Arabidopsis thaliana* Ler-0 epidermal cells infected by mature biotrophic hyphae (BH) of *C. higginsianum*. The host plasma membrane (HP) and tonoplast (T) are both intact, but the host cytoplasm shows major changes in ultrastructure suggestive of autophagy. **A,** Transverse sections through biotrophic hyphae located close to the host cell wall (HW) or **B,** crossing the host cell lumen and surrounded by a layer of host cytoplasm. Numerous small vacuole-like compartments (asterisks) and membrane whorls resembling autophagosomes (large arrowheads) are visible in the host cytoplasm. **C to E,** Higher-magnification views of three autophagosome-like structures bounded by double-layer membranes, some containing smaller membranous compartments and whorls. A, autophagosome; V, host vacuole; T, tonoplast; FW, fungal cell wall. **F,** Anti-GFP (green fluorescent protein) immunoblot of protein extracts from 7-day-old *pUBQ10::GFP-ATG8a Arabidopsis* seedlings either mock inoculated or infected with *C. higginsianum* at 24, 48, 52, 56, and 60 h postinoculation (hpi). Arrows identify GFP-ATG8a and free GFP released by proteolysis. **G**, Densitometric semiquantification of the autophagy flux, defined as the band intensity of full-length GFP-ATG8a divided by the band intensity of free GFP at each time point of *C. higginsianum* infection. The graph represents data from five independent biological replicates. One-way analysis of variance revealed statistically significant differences in autophagy flux at the five tested time points $F_{(4, 16)} = 2.429$, $P = 0.0231$. Post hoc Tukey's honestly significant difference test for multiple comparisons found that the mean autophagy flux was significantly different between 24 to 48 ($P = 0.0296$), 48 to 52 ($P = 0.0154$), and 24 to 52 ($P = 0.00032$) hpi.

of GFP-ATG8a to free GFP was calculated using densitometry, which showed that autophagic flux has an overall increasing trend during infection (Fig. 3G).

Late biotrophic and necrotrophic phase

By 55 hpi, *C. higginsianum* formed branched, multiseptate hyphae (Fig. 4; Supplementary Video S8). Figure 4A and B shows the first and 300th image from a single SBF-SEM image stack. The first image shows a single branched hypha with one septum, while the second image appears to show three separate hyphae. Only by reconstructing the 3D volume can one discern that the latter image represents three branches of a single hypha. These images also reveal that the vacuolar membrane has ruptured at this stage; however, the hyphae have not yet entered adjacent cells. The underlying mesophyll cells appear undamaged, as the chloroplasts, tonoplast, and the PM in the mesophyll cells all appear intact, with the chloroplasts located at the periphery of these cells (Supplementary Video S8), similar to what was seen at previous stages of the infection process (Supplementary Videos S1 to S7). We again manually segmented the infected host cell, the fungal hypha, and some of the membrane-bound bodies throughout the imaging volume (colored light blue in Fig. 4C and D and Supplementary Video S9), and using isosurface modeling, we found that there was extensive host membrane fragmentation in the infected cells at this stage (Supplementary Video S10).

At 60 hpi, the fungus had differentiated thinner secondary necrotrophic hyphae from the tips of the biotrophic hyphae, and these had successfully penetrated the epidermal cell walls to invade neighboring cells and intercellular spaces (Fig. 5A). Often, we found osmiophilic particles in the intercellular spaces near necrotrophic hyphae using both TEM (Fig. 5B, B1), serial section TEM (Fig. 5C, C1 to C3), and SBF-SEM (Fig. 5A; Supplementary Video S11). The mean diameter of these particles was measured to be 222.61 ± 1.84 nm (mean ± SE). Their dark staining suggests that these particles contain lipids; we thus speculate that these may represent extracellular vesicles being released by the host cells as a part of an unsuccessful immune response.

Complete withdrawal of the PM from the cell wall was evident in the first-infected host epidermal cell at 60 hpi (Fig. 5A; Supplementary Videos S11 and S13). Furthermore, membranes and chloroplasts in the subepidermal mesophyll cells had also completely degenerated (Fig. 5A; Supplementary Video S11), suggesting that *C. higginsianum* had successfully transitioned into full-fledged necrotrophy. Of note, the multinucleate necrotrophic mycelium (Supplementary Video S11) was found

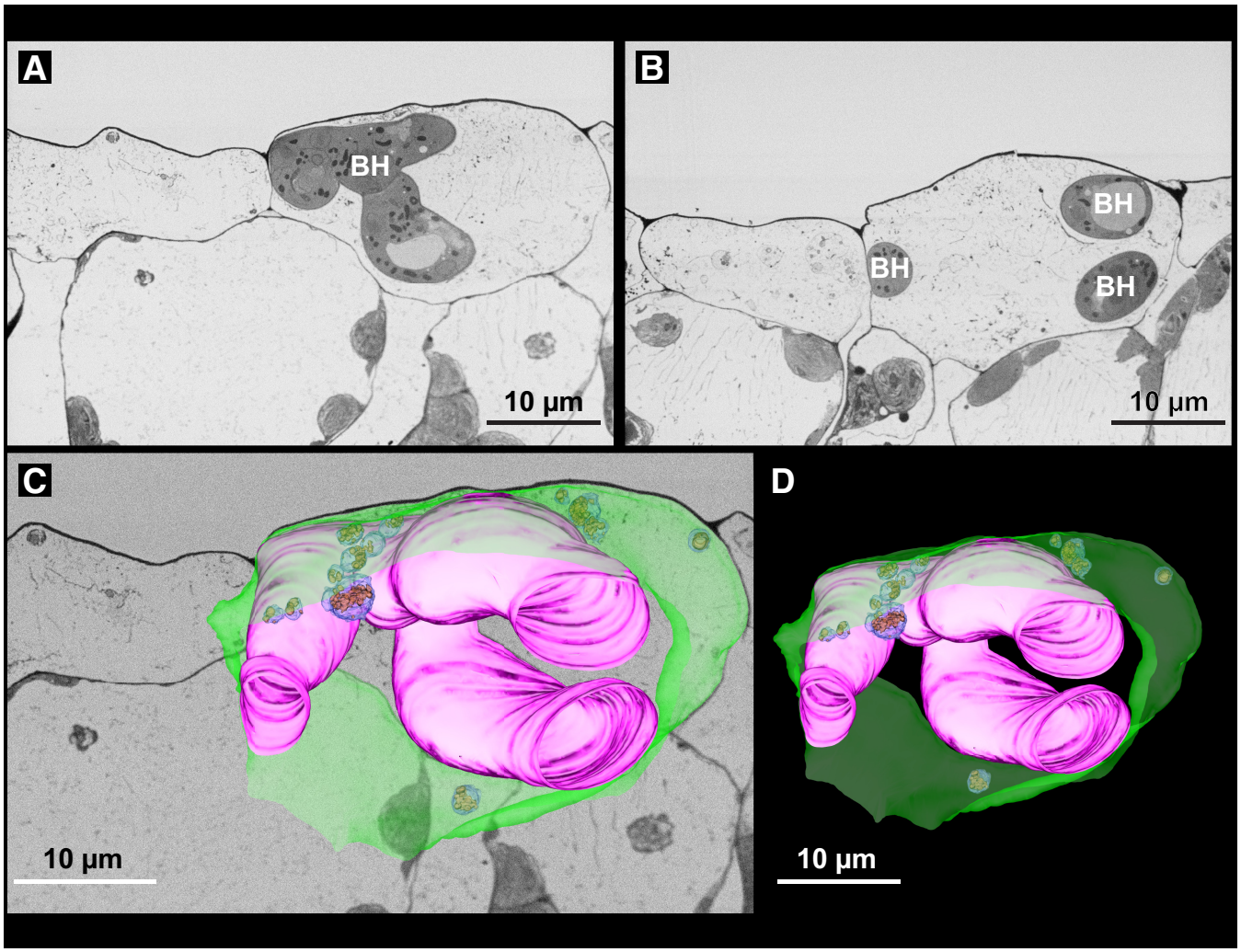

Fig. 4. Tonoplast fragmentation during *Colletotrichum higginsianum* infection of Col-0 at 55 h postinoculation (hpi). **A and B,** The 1st and 300th serial block-face scanning electron microscopy (SBF-SEM) micrographs from a single image stack showing late biotrophic hyphae (BH) at 55 hpi and total vacuolar disintegration. **C and D,** A 3D reconstruction from this image stack showing that hyphae are multilobed (magenta). Multiple membrane-bound bodies (light blue) containing electron-dense bodies (light brown) close to the multilobed hyphae are also depicted. Please refer to Supplementary Videos S6 and S7 for full isosurface renderings, which illustrate the high level of vacuolar fragmentation at this late biotrophic stage.

to form a single branched, multiseptate superstructure when reconstructed in 3D (Fig. 5D and E; Supplementary Video S12). By comparison, the mock-inoculated control (i.e., water droplet for 60 h) showed no such membrane disruption (Supplementary Video S14), confirming that the membrane disruption observed in the infected cells was pathogen induced.

Discussion

Using SBF-SEM, this study provides a collection of 3D ultrastructural views of the pathogenesis of the hemibiotrophic fungal pathogen *C. higginsianum* in *Arabidopsis* cotyledons. Upon successful penetration into the epidermal cells, *C. higginsianum* formed globular biotrophic hyphae by 52 hpi, which were surrounded by an intact host PM (Figs. 1B and 2A; Supplementary Videos S1 to S4). During this transient biotrophic phase, the structural integrity of the host cell membranes, including the tonoplast and PM, and organellar membrane was maintained (Figs. 1B and G and 2A; Supplementary Videos S1, S4, and S6). By extension, the host cell was still alive. Compared with prior ultrastructural studies of *Colletotrichum* infection sites (Mims and Vaillancourt 2002; O'Connell et al. 1985, 2004; Wharton et al. 2001; Xuei et al. 1988), our work has provided a more comprehensive picture of the extent of host cell membrane remodeling during each stage of the infection process. In particular, our 3D models revealed extensive branching of biotrophic hyphae within epidermal cells that largely replace the volume occupied by the central vacuole. To accommodate this large volume of fungal hyphae, both the PM and tonoplast membrane must undergo a massive increase in surface area, which in turn must require an increase in lipid biosynthesis. Consistent with this conclusion, a recent transcriptome analysis of tea leaves

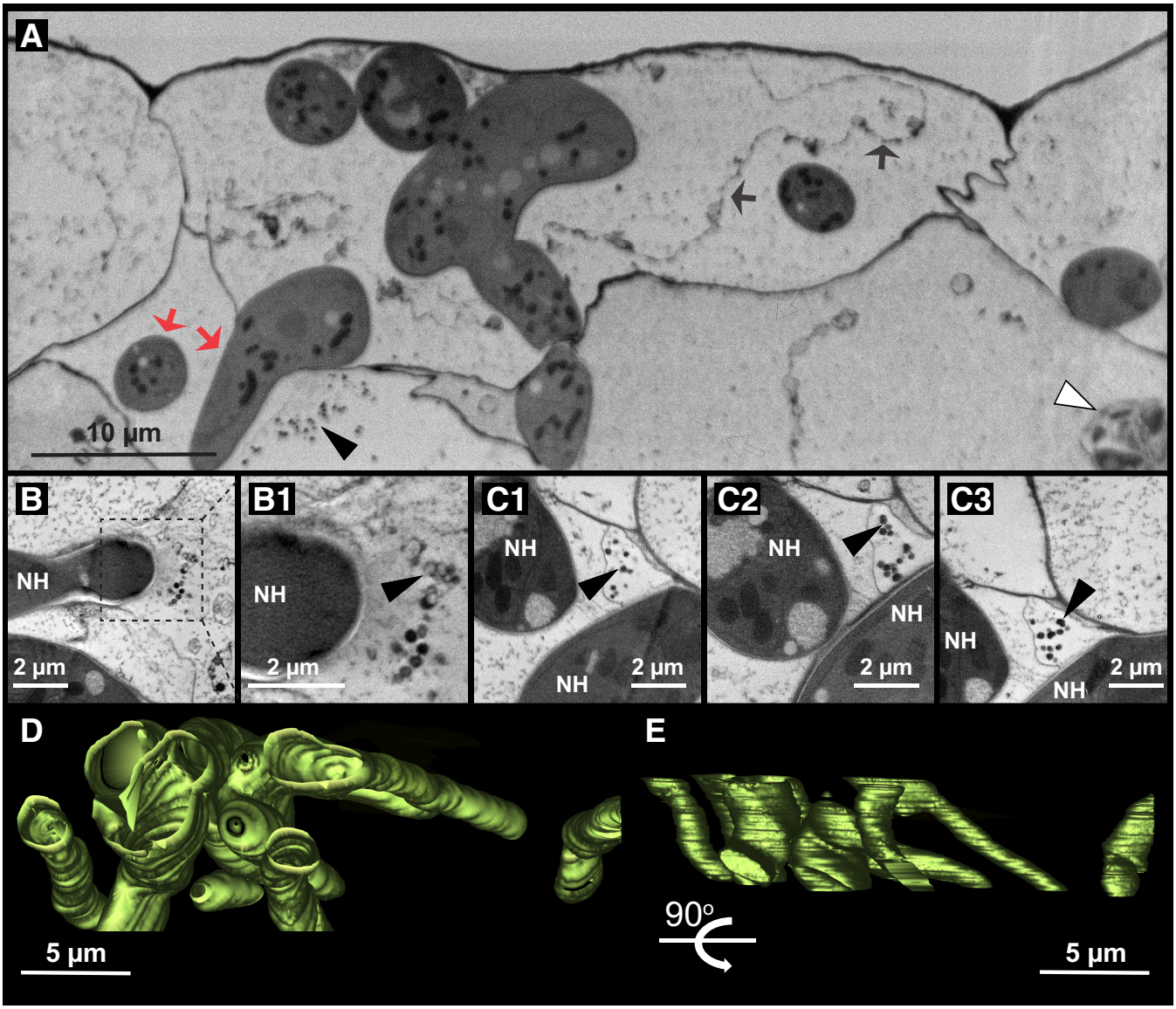

Fig. 5. Proliferating necrotrophic hypha form a single interconnected superstructure by 60 h postinoculation (hpi). **A,** The 120th micrograph from an serial block-face scanning electron microscopy (SBF-SEM) image stack containing 300 images showing the proliferation of necrotrophic fungal hyphae at 60 hpi. The plasma membrane (black arrows) has retracted from the cell wall, and the chloroplast in the mesophyll has swollen and appears to be disintegrating (white arrowhead). Osmiophilic particles are also observed in the intercellular space (black arrowhead), as are fungal hyphae (red arrows). **B,** Electron micrograph showing a necrotrophic hypha (NH) with the boxed region, **B1,** showing a higher-magnification view of proximally located osmiophilic bodies (arrowhead). **C1 to C3,** Serial section transmission electron micrographs showing osmiophilic bodies (arrowheads) in the vicinity of necrotrophic hyphae (NH). **D,** A 3D reconstruction of the necrotrophic hypha from 300 micrographs reveals that the hypha is an integrated superstructure (light green). **E,** The 3D model from D rotated 90°. Please refer to Supplementary Videos S11 to S13 for full movies.

infected with *Colletotrichum camelliae* revealed a strong upregulation of genes associated with lipid biosynthesis (Liu et al. 2023).

To confirm that this is also the case in *Arabidopsis*, we analyzed previously published RNA sequencing (RNA-Seq) data from *Arabidopsis* leaves infected with *C. higginsianum* (O'Connell et al. 2012). This dataset included RNA-Seq analysis of RNA isolated from *Arabidopsis* epidermal cells at 22 hpi (before host cell penetration) and at 40 hpi (biotrophic hyphae formation). Reasoning that host lipid biosynthesis requirements would be higher at 40 hpi than at 22 hpi, we thus selected genes that were upregulated at least twofold at the latter time point relative to the former. KEGG pathway enrichment analysis on this subset of *Arabidopsis* genes using ShinyGO 0.77 (Ge et al. 2020) revealed that glycerophospholipid metabolism is indeed significantly enriched (Supplementary Table S1), consistent with our conclusion that lipid biosynthesis must be increased dramatically in infected cells.

The conclusion that there is a large increase in membrane biosynthesis is also supported by previous confocal analyses of *C. higginsianum* infecting transgenic *Arabidopsis* plants expressing GFP-PEN1 (Shimada et al. 2006). PEN1 is a syntaxin protein that localizes to early endosomes and the PM. The images in Shimada et al. (2006) (their Figure 7) show that the GFP-PEN1 signal invaginates around biotrophic hyphae as they emerge from the appressoria, but then fade as the hyphae elongate, suggesting that the membrane surrounding the growing hyphae is being actively synthesized and excludes PEN1.

Although we observed a large increase in host cell PM during the biotrophic phase of *C. higginsianum* infection, we noted that the interfacial matrix layer between the host cell PM and biotrophic hyphae was quite thin (Fig. 1; Supplementary Video S1). A relatively thin interfacial matrix in this pathosystem has been documented previously (Kleemann et al. 2012) and is similar to that described in infections of rice leaf sheath epidermal cells by *Magnaportha oryzae* (Kankanala et al. 2007). But these observations contrast with a thicker inferfacial matrix observed in *C. sublineola*-infected sorghum leaf sheath (Wharton et al. 2001) and *C. graminicola*-infected maize leaves (Mims and Vaillancourt 2002). It also contrasts with relatively thick interfacial matrices observed surrounding haustoria of biotrophic pathogens such as flax rust, powdery mildew, and *Albugo candida* (Littlefield and Bracker 1972; Micali et al. 2011; Woods and Gay 1983). More recently, electron tomography studies have shown that the symbiotic interfaces between *Rhizophagus irregularis* in the roots of *Medicago truncatula* (Ivanov et al. 2019) and *Oryza sativa* (Roth et al. 2019) have extensive arbuscular tubules and that the intervening spaces have an abundance of vesicles. We observed similar vesiculo-tubular structures adjacent to necrotrophic hyphae, often in extracellular spaces (Fig. 5; Supplementary Video S12), suggesting that plants and/or fungi are releasing vesicles during the infection process, especially by the onset of necrotrophy.

Notably, we also observed cigar-shaped structures reminiscent of ER bodies in proximity to the biotrophic hyphae (Fig. 1D; Supplementary Video S3) that, when modeled in 3D, appeared to be interconnected in stacks (Fig. 1E; Supplementary Video S2). In Brassicaceae plants such as *Arabidopsis*, spindle-shaped ER bodies are distributed in epidermal cells of cotyledons and hypocotyls and are induced by wounding and methyl jasmonate. They are highly enriched in β-glucosidases that are known to hydrolyze glucosinolates to release isothiocyanates (Geem et al. 2019; Gunning 1998; Hayashi et al. 2001; Matsushima et al. 2002, 2003b; Nakazaki et al. 2019; Rufián et al. 2021; Stefanik et al. 2020; Yamada et al. 2020). ER bodies are thus thought to play an important role in defense against insects and fungi in the Brassicaceae. To confirm that these structures were likely ER bodies, we performed confocal analysis of *Arabidopsis* cotyledon epidermal cells expressing an ER-localized GFP infected with *C. higginsianum* (Supplementary Fig. S1). These images showed a clear accumulation of ER bodies surrounding fungal penetration sites, indicating that ER bodies contribute to the defense response against *C. higginsianum.*

In addition to ER bodies, our imaging revealed evidence of autophagy being induced by *C. higginsianum* infection. Autophagy in plants can be classified into three non-mutually exclusive categories, namely, microautophagy, macroautophagy, and megaautophagy (Hiratsuka and Terasaka 2011; Marshall and Vierstra 2018; van Doorn and Papini 2013; van Doorn et al. 2011). Macroautophagy, the most studied form of autophagy, is characterized by the formation of a double-membrane structure, the autophagosome, which engulfs part of the cytoplasm before merging with the lysosomal vacuole. ATG8 is a key protein involved in autophagosome maturation and function and is thought to mediate selective autophagy of target substrates (Chen et al. 2019; Marshall and Vierstra 2018; Nakatogawa et al. 2007; Ohsumi 2001; Woo et al. 2014; Xie et al. 2008). Autophagy has been observed during plant immune responses, but it is unclear whether autophagy functions to defend plants from pathogens, or whether pathogens manipulate host autophagy to promote infection. Defense-related autophagosomes labeled by GFP-ATG8 were reported to be frequently concentrated around the haustoria formed by the hemibiotrophic oomycete *Phytophthora infestans* in *Nicotiana tabacum* cells (Dagdas et al. 2018). On the other hand, Pandey and colleagues present evidence that autophagy triggered by the effector PexRD54 is beneficial to the oomycete, because starvation-induced autophagy might facilitate nutrient uptake from host cells (Pandey et al. 2021).

During the mid/late biotrophic phase (24 to 56 hpi), we observed autophagosomes in epidermal cells clustered near biotrophic hyphae (Fig. 3A to E), concurrent with an increase in autophagic flux (Fig. 3F and G), which suggests that either infected plant cells deploy defense-related autophagosomes toward the pathogenic hyphae or that these autophagosomes are induced by starvation and assist pathogen nutrition instead. How autophagosomes play a defensive role at this stage of infection remains unclear; some possibilities include degrading of fungal effectors in a process reminiscent of xenophagy, recycling and remobilization of plant resources to produce immune-related proteins and structures or mediating unconventional secretion of immune-related proteins or vesicles (Xu et al. 2019). Alternatively, the profusion of autophagosomes in proximity to the *C. higginsianum* biotrophic hyphae may represent a way in which the plant membrane trafficking is manipulated by the pathogen.

Overall, the use of SBF-SEM allowed us to document the ultrastructure of *C. higginsianum* infection in *Arabidopsis* cotyledons much more efficiently than conventional serial-section TEM. In particular, the ability to generate hundreds of serial sections in an automated manner enabled us to quickly identify rare sections that are highly informative, such as sections showing penetration pegs (Fig. 1B), hyphal branch points (Fig. 4A), or hyphae emerging from epidermal cells into the extracellular space (Fig. 5A). More significantly, these stacks of serial sections enabled generation of 3D models that allowed us to more fully understand the hyphal morphology as the disease progressed from biotrophy to necrotrophy. Specifically, we were able to visualize how the bulbous hypha in the biotrophic stage transforms into a multilobed structure that, in turn, metamorphoses into an integrated superstructure upon reaching necrotrophy. Concomitant with the growth of the fungal hyphae, we were able to visualize large changes in host cell membranes, marked first by dramatic expansion of the PM and tonoplast, and followed by fragmentation of the central vacuole and, ultimately, rupture of the central vacuole. The fragmentation of the central vacuole was made es-

pecially obvious using the isosurface modeling tool provided by the IMOD software (Supplementary Video S7). Such analyses are not possible with a limited number of sections typically obtained using standard TEM.

Materials and Methods

Fungal cultures

Colletotrichum higginsianum isolate IMI349063A was used in this study. Stocks of fungal spores were stored in 15% glycerol and 1X potato dextrose broth at –80°C, and cultures were prepared fresh from glycerol stocks and grown on Petri dishes on solid Mathur's medium (2.8 g/liter of glucose, 2.2 g/liter of mycological peptone, 0.5 g/liter of yeast extract, 1.2 g/liter of $MgSO_4x7H_2O$, 2.7 g/liter of KH_2PO_4, 20 g/liter of agar, pH 5.5). The cultures were allowed to grow for 3 weeks in a short-day growth room equipped with GE HI-LUMEN XL Starcoat 32-watt fluorescent bulbs (a 50:50 mixture of 3,500- and 5,000-K spectrum bulbs) with 9-h days, 22°C, 150 μE/m^2/s. To harvest the spores, ~2 ml of sterile water was applied to the surface of 3-week-old plate cultures, and the surface was scraped using a sterilized glass rod. The spore suspension was transferred to an Eppendorf tube and washed three times by pelleting at 2,000 × *g* for 5 min and resuspension of the pelleted spores in sterile water. The spore concentration was then adjusted to 2×10^6 spores/ml using a Neubauer chamber.

Plant growth and spot inoculation

Arabidopsis thaliana ecotype Col-0 seeds were sterilized and plated on solid one-half MS medium in Petri plates and stratified at 4°C in the dark for 48 h before being transferred to a short-day growth room equipped with GE HI-LUMEN XL Starcoat 32-watt fluorescent bulbs (a 50:50 mixture of 3,500- and 5,000-K spectrum bulbs) with 9-h days, 22°C, 150 μE/m^2/s. Seven days after germination, each cotyledon was spot-inoculated with ~2 μl of 2×10^6 spores/ml of *C. higginsianum* spores and incubated in the dark for 12 h at room temperature in the same Petri plate sealed with micropore tape (3M), before being transferred to the short-day room until HPF. As mock-inoculation controls, ~2 μl of sterile water was spotted onto each of the cotyledons instead. Even after 60 h of incubation, the water droplet had not evaporated, indicating that the sealed Petri plates maintained near 100% humidity.

High-pressure freezing, freeze-substitution, and resin embedding

At 52, 55, or 60 hpi, any remaining water on cotyledons was wicked off with a Kim-wipe, whole cotyledons were detached with a double-edged razor and immediately transferred to a Type-B brass planchet containing 1-hexadecene, covered with another brass planchet (flat side down), and frozen using a Wohlwend HPF Compact 03 high-pressure freezer. The planchets were then transferred to a cryotube containing precooled (–80°C) freeze-substitution cocktail composed of 2% (wt/vol) OsO_4 in acetone. The samples were allowed to freeze-substitute for 48 h in a –80°C freezer, and then were transferred to a –20°C freezer for 4 h, followed by 2-hour incubation at 4°C under shaking. Finally, the samples were warmed to room temperature in a fume hood for 1 h with shaking. The samples were washed with fresh acetone five times for 10 min each wash, then transferred to a freshly prepared mordant solution containing 0.3% (wt/vol) thiocarbohydrazide in acetone and incubated for 1 h under rotation at room temperature. The samples were washed with fresh acetone five times for 10 min each wash, and incubated with 2% OsO_4 (wt/vol) in acetone for 2 h at room temperature. The samples were again washed five times (10 min each) with fresh acetone before en bloc staining with 0.2% (wt/vol) uranyl acetate in acetone overnight at 4°C. The samples were again washed with fresh acetone five times for 10 min each wash, before gradual infiltration with Durcupan resin in 10%, 25%, 50%, 75%, and 5 × 100% resin over a period of 3 days. During each of the 100% resin infiltration steps, samples were carefully layered on top of fresh resin and centrifuged at 2,000 rpm until the samples reached the bottom of the 2 ml centrifuge tubes (usually ~2 min) (McDonald 2014). Finally, the samples were flat-embedded in Durcupan using Aclar (Kingsley and Cole 1988) or flat-embedding molds in an oven at 60°C.

Sample preparation and evaluation for SBF-SEM

The resin-embedded samples were first roughly trimmed using a jeweler's saw and mounted on aluminum stubs using EPO-TEK electrically conductive resin, and the substrate was allowed to solidify in an oven set at 60°C overnight. The resin-embedded samples were trimmed by hand using a double-edged razor blade to an approximate height of 0.5 mm, length of 2 mm, and width of 300 μm; sputter-coated with 45-nm 80:20 Au:Pd at 3.8×10^{-2} Torr and 30 mA (Safematic CCU-010 Compact Coating Unit), before the block-face was smoothed with a diamond knife (Diatome) using a Leica Ultracut ultramicrotome. Semi-thin sections (~300 to 500 nm) were collected and stained with epoxy staining solution (EMSdiasum) for observation under a light microscope or ultrathin (~90 nm) sections were picked up on copper slot grids for evaluation using a JEOL JEM 1010 transmission electron microscope operating at 80 kV. No poststaining was done before observation using TEM. For conventional TEM shown in Figure 3, leaves of 4-week-old *A. thaliana* Ler-0 plants were inoculated with droplets (2 μl) of *C. higginsianum* spore suspension (5×10^5/ml). At 22 hpi, disks of tissue were removed from beneath the inoculation sites using a 2-mm biopsy punch and prepared by HPF, freeze-substitution, and embedding in epoxy resin, as described by Micali et al. (2011). Ultrathin (90-nm) sections were collected on copper slot grids and stained with 1% (wt/vol) potassium permanganate for 1 min or 2% (wt/vol) uranyl acetate for 10 min, followed by lead citrate for 15 min, before observation with a Hitachi H-7650 TEM operating at 100 kV.

SBF-SEM

The samples were imaged using an FEI Teneo VolumeScope (ThermoFisher) equipped with an in situ ultramicrotome. The blocks were sectioned at 40-nm thickness, and images were obtained at 2.5 kV/0.8 nA at a low vacuum pressure of 50 Pa. Each image was 6,144 × 4,096 pixels with *x-y* pixel size of 10 nm. The serial images were first batch-inverted using Adobe Photoshop CC and then processed using IMOD (Kremer et al. 1996) to perform segmentation, isosurface rendering, and 3D reconstructions. Supplementary Videos were created from serial images using Adobe Photoshop CC or QuickTime Player. Before isosurface modeling, the images were compressed fourfold (i.e., 1,536 × 1,024 pixels) to increase the volume of the bounding box. The mean diameter of the osmiophilic particles observed in Figure 5C and Supplementary Video S11 were manually measured in Fiji from a total of 1,281 particles from 50 SBF-SEM images.

Confocal microcopy

For confocal microscopy of ER bodies, 12-day-old seedlings of *A. thaliana* Col-0 expressing GFP fused with an ER retention signal (p35s::sp-gfp-hdel, Matsushima et al. 2003b) were spray-inoculated with spore suspension of *C. higginsianum* (5×10^5/ml) and incubated in a humid chamber at 25°C. Hypocotyl and cotyledon tissues were mounted in water and examined using a Leica TCS SP2 confocal microscope (Leica Microsystems) equipped with an APO 63× (1.20 NA) water-immersion objec-

tive. GFP was excited using the 488-nm laser lines, and images were processed with Lecia LAS-X and ImageJ software.

Autophagic flux assay

Arabidopsis line *pUBQ10::GFP-ATG8a* was acquired from the Arabidopsis Biological Resource Center (ABRC) at the Ohio State University. These seedlings were germinated and grown on one-half MS Petri plates and spot-inoculated with 2×10^6 spores as described earlier. Eight seedlings per time point were frozen in liquid nitrogen and ground with a mortar and pestle on ice. To extract protein, ground tissue was mixed and vortexed in cold buffer containing 150 mM NaCl, 50 mM Tris HCl pH 7.5, 0.1% (vol/vol) NP40, and 1% (wt/vol) protease inhibitor cocktail (Sigma catalog no. P9599). After a 5-min incubation on ice, debris was pelleted at 16,000 × *g*. Protein concentration of the supernatant was determined using the Pierce 660 assay (ThermoFisher catalog no. 22660). Equal amounts of protein for each time point were mixed with 5X loading dye containing 250 mM Tris-HCl pH 6.8, 10% wt/vol sodium dodecyl sulfate, 40% vol/vol glycerol, 20% vol/vol β-mercaptoethanol, and 0.02% bromophenol blue, and boiled at 95°C for 5 min. Samples were loaded into 4 to 20% denaturing polyacrylamide gel (Bio-Rad catalog no. 456-8094) and transferred to nitrocellulose membranes using a semi-dry system (Bio-Rad no. 170-3940). After blocking overnight in 5% wt/vol Difco skim milk (BD no. 232100) in Tris-buffered saline with 0.1% Tween-20 at 4°C, membranes were probed with anti-GFP horseradish peroxidase (Abcam catalog no. 6663) diluted 1:5,000 in blocking buffer for 1 h at room temperature. After washing, ECL substrate (Bio-Rad catalog no. 1705061) was applied and chemiluminescence detected using a ChemiDoc (Bio-Rad catalog no. 12003154). Immunoblot band intensities were measured using Fiji, and statistical analyses were performed in GraphPad Prism.

Acknowledgments

We thank the IU Bloomington Electron Microscopy Center at Indiana University for access to the Wohlwend HPF Compact 03 high-pressure freezer, Leica Ultracut ultramicrotome, JEOL JEM 1010 Transmission Electron Microscope, and FEI Teneo VolumeScope, and we thank IUB-EMC staff member Barry Stein for assistance with using this equipment.

Author-Recommended Internet Resource

IMOD home page: https://bio3d.colorado.edu/imod

Literature Cited

Bailey, J. A., O'Connell, R. J., Pring, R. J., and Nash, C. 1992. Infection strategies of *Colletotrichum* species. Pages 88-120 in: *Colletotrichum*: Biology, Pathology and Control. J. A. Bailey and M. J. Jeger eds. CAB International, Wallingford, U.K.

Bassham, D. C. 2015. Methods for analysis of autophagy in plants. Methods 75:181-188.

Brown, G. E. 1977. Ultrastructure of penetration of ethylene-degreened robinson tangerines by *Colletotrichum gloeosporioides*. Phytopathology 67:315-320.

Chen, Q., Soulay, F., Saudemont, B., Elmayan, T., Marmagne, A., and Masclaux-Daubresse, C. 2019. Overexpression of *ATG8* in Arabidopsis stimulates autophagic activity and increases nitrogen remobilization efficiency and grain filling. Plant Cell Physiol. 60:343-352.

Crous, P. W., Gams, W., Stalpers, J. A., Robert, V., and Stegehuis, G. 2004. MycoBank: An online initiative to launch mycology into the 21st century. Stud. Mycol. 50:19-22.

Dagdas, Y. F., Belhaj, K., Maqbool, A., Chaparro-Garcia, A., Pandey, P., Petre, B., Tabassum, N., Cruz-Mireles, N., Hughes, R. K., Sklenar, J., Win, J., Menke, F., Findlay, K., Banfield, M. J., Kamoun, S., and Bozkurt, T. O. 2016. An effector of the Irish potato famine pathogen antagonizes a host autophagy cargo receptor. eLife 5:e10856.

Dagdas, Y. F., Pandey, P., Tumtas, Y., Sanguankiattichai, N., Belhaj, K., Duggan, C., Leary, A. Y., Segretin, M. E., Contreras, M. P., Savage, Z., Khandare, V. S., Kamoun, S., and Bozkurt, T. O. 2018. Host autophagy machinery is diverted to the pathogen interface to mediate focal defense responses against the Irish potato famine pathogen. eLife 7: e37476.

Denk, W., and Horstmann, H. 2004. Serial block-face scanning electron microscopy to reconstruct three-dimensional tissue nanostructure. PLoS Biol. 2:e329.

Faoro, F., Faccio, A., and Balestrini, R. 2022. Contributions of ultrastructural studies to the knowledge of filamentous fungi biology and fungi-plant interactions. Front. Fungal Biol. 2:805739.

Ge, S. X., Jung, D., and Yao, R. 2020. ShinyGO: A graphical gene-set enrichment tool for animals and plants. Bioinformatics 36:2628-2629.

Geem, K. R., Kim, D. H., Lee, D. W., Kwon, Y., Lee, J., Kim, J. H., and Hwang, I. 2019. Jasmonic acid-inducible TSA1 facilitates ER body formation. Plant J. 97:267-280.

Gunning, B. E. S. 1998. The identity of mystery organelles in *Arabidopsis* plants expressing GFP. Trends Plant Sci. 3:417.

Hane, J. K., Paxman, J., Jones, D. A. B., Oliver, R. P., and de Wit, P. 2020. "CATAStrophy," a genome-informed trophic classification of filamentous plant pathogens—how many different types of filamentous plant pathogens are there? Front. Microbiol. 10:03088.

Hayashi, Y., Yamada, K., Shimada, T., Matsushima, R., Nishizawa, N. K., Nishimura, M., and Hara-Nishimura, I. 2001. A proteinase-storing body that prepares for cell death or stresses in the epidermal cells of Arabidopsis. Plant Cell Physiol. 42:894-899.

Heath, M. C. 1983. Relationship between developmental stage of the bean rust fungus and increased susceptibility of surrounding bean tissue to the cowpea rust fungus. Physiol. Plant Pathol. 22:45-50.

Hiratsuka, R., and Terasaka, O. 2011. Pollen tube reuses intracellular components of nucellar cells undergoing programmed cell death in *Pinus densiflora*. Protoplasma 248:339-351.

Hiratsuka, R., Yamada, Y., and Terasaka, O. 2002. Programmed cell death of *Pinus* nucellus in response to pollen tube penetration. J. Plant Res. 115:0141-0148.

Ivanov, S., Austin, J., II, Berg, R. H., and Harrison, M. J. 2019. Extensive membrane systems at the host–arbuscular mycorrhizal fungus interface. Nat. Plants 5:194-203.

Kankanala, P., Czymmek, K., and Valent, B. 2007. Roles for rice membrane dynamics and plasmodesmata during biotrophic invasion by the blast fungus. Plant Cell 19:706-724.

Kingsley, R. E., and Cole, N. L. 1988. Preparation of cultured mammalian cells for transmission and scanning electron microscopy using aclar film. J. Electron Microsc. Tech. 10:77-85.

Kleemann, J., Rincon-Rivera, L. J., Takahara, H., Neumann, U., van Themaat, E. V. L., van der Does, H. C., Hacquard, S., Stüber, K., Will, I., Schmalenbach, W., Schmelzer, E., and O'Connell, R. J. 2012. Sequential delivery of host-induced virulence effectors by appressoria and intracellular hyphae of the phytopathogen *Colletotrichum higginsianum*. PLoS Pathog. 8:e1002643.

Klionsky, D. J., Abdel-Aziz, A. K., Abdelfatah, S., Abdellatif, M., Abdoli, A., Abel, S., Abeliovich, H., Abildgaard, M. H., Abudu, Y. P., Acevedo-Arozena, A., Adamopoulos, I. E., Adeli, K., Adolph, T. E., Adornetto, A., Aflaki, E., Agam, G., Agarwal, A., Aggarwal, B. B., Agnello, M., Agostinis, P., Agrewala, J. N., Agrotis, A., Aguilar, P. V., Ahmad, S. T., Ahmed, Z. M., Ahumada-Castro, U., Aits, S., Aizawa, S., Akkoc, Y., Akoumianaki, T., Akpinar, H. A., Al-Abd, A. M., Al-Akra, L., Al-Gharaibeh, A., Alaoui-Jamali, M. A., Alberti, S., Alcocer-Gómez, E., Alessandri, C., Ali, M., Alim Al-Bari, M. A., et al. 2021. Guidelines for the use and interpretation of assays for monitoring autophagy (4th edition). Autophagy 17:1-382.

Kremer, J. R., Mastronarde, D. N., and McIntosh, J. R. 1996. Computer visualization of three-dimensional image data using IMOD. J. Struct. Biol. 116:71-76.

Latunde-Dada, A. O., O'Connell, R. J., Nash, C., Pring, R. J., Lucas, J. A., and Bailey, J. A. 1996. Infection process and identity of the hemibiotrophic anthracnose fungus (*Colletotrichum destructivum*) from cowpea (*Vigna unguiculata*). Mycol. Res. 100:1133-1141.

Littlefield, L. J., and Bracker, C. E. 1972. Ultrastructural specialization at the host-pathogen interface in rust-infected flax. Protoplasma 74:271-305.

Liu, F., Ma, Z. Y., Hou, L. W., Diao, Y. Z., Wu, W. P., Damm, U., Song, S., and Cai, L. 2022. Updating species diversity of *Colletotrichum*, with a phylogenomic overview. Stud. Mycol. 101:1-56.

Liu, S., Zhang, S., He, S., Qiao, X., and Runa, A. 2023. Tea plant (*Camellia sinensis*) lipid metabolism pathway modulated by tea field microbe (*Colletotrichum camelliae*) to promote disease. Hortic. Res. 10:uhad028.

Luttrell, E. S. 1974. Parasitism of fungi on vascular plants. Mycologia 66: 1-15.

Marshall, R. S., and Vierstra, R. D. 2018. Autophagy: The master of bulk and selective recycling. Annu. Rev. Plant Biol. 69:173-208.

Matsushima, R., Hayashi, Y., Kondo, M., Shimada, T., Nishimura, M., and Hara-Nishimura, I. 2002. An endoplasmic reticulum-derived structure that is induced under stress conditions in Arabidopsis. Plant Physiol. 130:1807-1814.

Matsushima, R., Hayashi, Y., Yamada, K., Shimada, T., Nishimura, M., and Hara-Nishimura, I. 2003a. The ER body, a novel endoplasmic reticulum-derived structure in *Arabidopsis*. Plant Cell Physiol. 44:661-666.

Matsushima, R., Kondo, M., Nishimura, M., and Hara-Nishimura, I. 2003b. A novel ER-derived compartment, the ER body, selectively accumulates a β-glucosidase with an ER-retention signal in *Arabidopsis*. Plant J. 33:493-502.

McDonald, K. L. 2014. Rapid embedding methods into epoxy and LR white resins for morphological and immunological analysis of cryofixed biological specimens. Microsc. Microanal. 20:152-163.

Micali, C. O., Neumann, U., Grunewald, D., Panstruga, R., and O'Connell, R. 2011. Biogenesis of a specialized plant–fungal interface during host cell internalization of *Golovinomyces orontii* haustoria. Cell. Microbiol. 13:210-226.

Mims, C. W., Richardson, E. A., Holt, B. F., III, and Dangl, J. L. 2004. Ultrastructure of the host pathogen interface in *Arabidopsis thaliana* leaves infected by the downy mildew *Hyaloperonospora parasitica*. Can. J. Bot. 82:1001-1008.

Mims, C. W., and Vaillancourt, L. J. 2002. Ultrastructural characterization of infection and colonization of maize leaves by *Colletotrichum graminicola*, and by a *C. graminicola* pathogenicity mutant. Phytopathology 92:803-812.

Mould, M. J. R., Boland, G. J., and Robb, J. 1991. Ultrastructure of the *Colletotrichum trifolii-Medicago sativa* pathosystem. II. Post-penetration events. Physiol. Mol. Plant Pathol. 38:195-210.

Nakatogawa, H., Ichimura, Y., and Ohsumi, Y. 2007. Atg8, a ubiquitin-like protein required for autophagosome formation, mediates membrane tethering and hemifusion. Cell 130:165-178.

Nakazaki, A., Yamada, K., Kunieda, T., Sugiyama, R., Hirai, M. Y., Tamura, K., Hara-Nishimura, I., and Shimada, T. 2019. Leaf endoplasmic reticulum bodies identified in Arabidopsis rosette leaves are involved in defense against herbivory. Plant Physiol. 179:1515-1524.

O'Connell, R. J. 1987. Absence of a specialized interface between intracellular hyphae of *Colletotrichum lindemuthianum* and cells of *Phaseolus vulgaris*. New Phytol. 107:725-734.

O'Connell, R. J., Bailey, J. A., and Richmond, D. V. 1985. Cytology and physiology of infection of *Phaseolus vulgaris* by *Colletotrichum lindemuthianum*. Physiol. Plant Pathol. 27:75-98.

O'Connell, R., Herbert, C., Sreenivasaprasad, S., Khatib, M., Esquerré-Tugayé, M.-T., and Dumas, B. 2004. A novel *Arabidopsis-Colletotrichum* pathosystem for the molecular dissection of plant-fungal interactions. Mol. Plant-Microbe Interact. 17:272-282.

O'Connell, R. J., Thon, M. R., Hacquard, S., Amyotte, S. G., Kleemann, J., Torres, M. F., Damm, U., Buiate, E. A., Epstein, L., Alkan, N., Altmüller, J., Alvarado-Balderrama, L., Bauser, C. A., Becker, C., Birren, B. W., Chen, Z., Choi, J., Crouch, J. A., Duvick, J. P., Farman, M. A., Gan, P., Heiman, D., Henrissat, B., Howard, R. J., Kabbage, M., Koch, C., Kracher, B., Kubo, Y., Law, A. D., Lebrun, M.-H., Lee, Y.-H., Miyara, I., Moore, N., Neumann, U., Nordström, K., Panaccione, D. G., Panstruga, R., Place, M., Proctor, R. H., Prusky, D., Rech, G., Reinhardt, R., Rollins, J. A., Rounsley, S., Schardl, C. L., Schwartz, D. C., Shenoy, N., Shirasu, K., Sikhakolli, U. R., Stüber, K., Sukno, S. A., Sweigard, J. A, Takano, Y., Takahara, H., Trail, F., van der Does, H. C., Voll, L. M., Will, I., Young, S., Zeng, Q., Zhang, J., Zhou, S., Dickman, M. B., Schulze-Lefert, P., Ver Loren van Themaat, E., Ma, L.-J., and Vaillancourt, L. J. 2012. Lifestyle transitions in plant pathogenic *Colletotrichum* fungi deciphered by genome and transcriptome analyses. Nat. Genet. 44:1060-1065.

Ohsumi, Y. 2001. Molecular dissection of autophagy: Two ubiquitin-like systems. Nat. Rev. Mol. Cell Biol. 2:211-216.

Pandey, P., Leary, A. Y., Tumtas, Y., Savage, Z., Dagvadorj, B., Duggan, C., Yuen, E. L. H., Sanguankiattichai, N., Tan, E., Khandare, V., Connerton, A. J., Yunusov, T., Madalinski, M., Mirkin, F. G., Schornack, S., Dagdas, Y., Kamoun, S., and Bozkurt, T. O. 2021. An oomycete effector subverts host vesicle trafficking to channel starvation-induced autophagy to the pathogen interface. eLife 10:e65285.

Roth, R., Hillmer, S., Funaya, C., Chiapello, M., Schumacher, K., Lo Presti, L., Kahmann, R., and Paszkowski, U. 2019. Arbuscular cell invasion coincides with extracellular vesicles and membrane tubules. Nat. Plants 5:204-211.

Rufián, J. S., Elmore, J. M., Bejarano, E. R., Beuzon, C. R., and Coaker, G. L. 2021. ER bodies are induced by *Pseudomonas syringae* and negatively regulate immunity. Mol. Plant-Microbe Interact. 34:1001-1009.

Shimada, C., Lipka, V., O'Connell, R., Okuno, T., Schulze-Lefert, P., and Takano, Y. 2006. Nonhost resistance in *Arabidopsis-Colletotrichum* interactions acts at the cell periphery and requires actin filament function. Mol. Plant-Microbe Interact. 19:270-279.

Shin, K. D., Lee, H. N., and Chung, T. 2014. A revised assay for monitoring autophagic flux in *Arabidopsis thaliana* reveals involvement of *AUTOPHAGY-RELATED9* in autophagy. Mol. Cells 37:399-405.

Stefanik, N., Bizan, J., Wilkens, A., Tarnawska-Glatt, K., Goto-Yamada, S., Strzałka, K., Nishimura, M., Hara-Nishimura, I., and Yamada, K. 2020. NAI2 and TSA1 drive differentiation of constitutive and inducible ER body formation in Brassicaceae. Plant Cell Physiol. 61:722-734.

Torggler, R., Papinski, D., and Kraft, C. 2017. Assays to monitor autophagy in *Saccharomyces cerevisiae*. Cells 6:23.

van Doorn, W. G., Beers, E. P., Dangl, J. L., Franklin-Tong, V. E., Gallois, P., Hara-Nishimura, I., Jones, A. M., Kawai-Yamada, M., Lam, E., Mundy, J., Mur, L. A. J., Petersen, M., Smertenko, A., Taliansky, M., Van Breusegem, F., Wolpert, T., Woltering, E., Zhivotovsky, B., and Bozhkov, P. V. 2011. Morphological classification of plant cell deaths. Cell Death Differ. 18:1241-1246.

van Doorn, W. G., and Papini, A. 2013. Ultrastructure of autophagy in plant cells: A review. Autophagy 9:1922-1936.

van Doorn, W. G., and Woltering, E. J. 2005. Many ways to exit? Cell death categories in plants. Trends Plant Sci. 10:117-122.

Voegele, R. T., and Mendgen, K. 2003. Rust haustoria: Nutrient uptake and beyond. New Phytol. 159:93-100.

Wharton, P. S., Julian, A. M., and O'Connell, R. J. 2001. Ultrastructure of the infection of *Sorghum bicolor* by *Colletotrichum sublineolum*. Phytopathology 91:149-158.

Woo, J., Park, E., and Dinesh-Kumar, S. P. 2014. Differential processing of *Arabidopsis* ubiquitin-like Atg8 autophagy proteins by Atg4 cysteine proteases. Proc. Natl. Acad. Sci. U.S.A. 111:863-868.

Woods, A. M., and Gay, J. L. 1983. Evidence for a neckband delimiting structural and physiological regions of the host plasma membrane associated with haustoria of *Albugo candida*. Physiol. Plant Pathol. 23:73-88.

Xie, Z., Nair, U., and Klionsky, D. J. 2008. Atg8 controls phagophore expansion during autophagosome formation. Mol. Biol. Cell 19:3290-3298.

Xu, Y., Zhou, P., Cheng, S., Lu, Q., Nowak, K., Hopp, A.-K., Li, L., Shi, X., Zhou, Z., Gao, W., Li, D., He, H., Liu, X., Ding, J., Hottiger, M. O., and Shao, F. 2019. A bacterial effector reveals the V-ATPase-ATG16L1 axis that initiates xenophagy. Cell 178:552-566.

Xuei, X. L., Järlfors, U., and Kuć, J. 1988. Ultrastructural changes associated with induced systemic resistance of cucumber to disease: Host response and development of *Colletotrichum lagenarium* in systemically protected leaves. Can. J. Bot. 66:1028-1038.

Yamada, K., Goto-Yamada, S., Nakazaki, A., Kunieda, T., Kuwata, K., Nagano, A. J., Nishimura, M., and Hara-Nishimura, I. 2020. Endoplasmic reticulum-derived bodies enable a single-cell chemical defense in Brassicaceae plants. Commun. Biol. 3:21.